Petroleum Science 21 (2024) 302–314

Contents lists available at ScienceDirect

Petroleum Science

journal homepage: www.keaipublishing.com/en/journals/petroleum-science

Original Paper

Liquid injectivity in a SAG foam process: Effect of permeability

Jia-Kun Gong [a, d, *], Yuan Wang [b], Ridhwan-Zhafri B. Kamarul Bahrim [c], Raj-Deo Tewari [c], Mohammad-Iqbal Mahamad Amir [c], Rouhi Farajzadeh [d, e], William Rossen [d]

[a] College of Mechanics and Materials, Hohai University, Nanjing, 210098, Jiangsu, China
[b] College of Water Conservancy & Hydropower Engineering, Hohai University, Nanjing, 210098, Jiangsu, China
[c] PETRONAS, Kuala Lumpur, 50088, Malaysia
[d] Department of Geoscience and Engineering, Delft University of Technology, 2628 CN, Delft, the Netherlands
[e] Shell Global Solutions International B.V., 1031 HW, Amsterdam, the Netherlands

ARTICLE INFO

Article history:
Received 6 June 2023
Received in revised form
12 October 2023
Accepted 12 October 2023
Available online 13 October 2023

Edited by Yan-Hua Sun

Keywords:
Foam
Enhanced oil recovery
Surfactant-alternating-gas
Injectivity
Permeability

ABSTRACT

Foam is utilized in enhanced oil recovery and CO_2 sequestration. Surfactant-alternating-gas (SAG) is a preferred approach for placing foam into reservoirs, due to it enhances gas injection and minimizes corrosion in facilities. Our previous studies with similar permeability cores show that during SAG injection, several banks occupy the area near the well where fluid exhibits distinct behaviour. However, underground reservoirs are heterogeneous, often layered. It is crucial to understand the effect of permeability on fluid behaviour and injectivity in a SAG process. In this work, coreflood experiments are conducted in cores with permeabilities ranging from 16 to 2300 mD. We observe the same sequence of banks in cores with different permeabilities. However, the speed at which banks propagate and their overall mobility can vary depending on permeability. At higher permeabilities, the gas-dissolution bank and the forced-imbibition bank progress more rapidly during liquid injection. The total mobilities of both banks decrease with permeability. By utilizing a bank-propagation model, we scale up our experimental findings and compare them to results obtained using the Peaceman equation. Our findings reveal that the liquid injectivity in a SAG foam process is misestimated by conventional simulators based on the Peaceman equation. The lower the formation permeability, the greater the error.
© 2023 The Authors. Publishing services by Elsevier B.V. on behalf of KeAi Communications Co. Ltd. This is an open access article under the CC BY-NC-ND license (http://creativecommons.org/licenses/by-nc-nd/4.0/).

1. Introduction

Gas injection is widely used as a technique for enhanced oil recovery due to its ability to retrieve nearly all oil through its sweeping action (Lake et al., 2014). However, gas often has poor gas sweep efficiency because of its low density and viscosity. The low gas density results in gas to flow towards the top of the reservoir, additionally, the low gas viscosity can lead to viscous instability and formation of high-mobility channels in the reservoir, leaving oil unrecovered. The gas sweep efficiency can be improved by foam, due to its capability in reducing gas gravity override and viscous fingering (Hirasaki and Lawson, 1985; Kovscek and Radke, 1994; Rossen, 1996; Farajzadeh et al., 2010) and the effect of formation heterogeneity on the injection profile (Moradi-Araghi et al., 1997; Farajzadeh et al., 2015). Therefore, foam is widely used in enhanced oil recovery (Li et al., 2023). Foam is also applied for aquifer remediation in a manner similar to the enhanced-oil-recovery process (Wang and Mulligan, 2004; Atteia et al., 2013).

There are two primary methods for placing foam into reservoirs: by co-injecting solution of surfactant and gas, and injecting alternatively surfactant and gas slugs, a process also known as SAG (Schramm, 1994; Kibodeaux and Rossen, 1997; Rossen et al., 2010). In addition, there are alternative techniques available for foam injection, including the process of incorporating surfactants into supercritical CO_2 through dissolution (Le et al., 2008; Xing et al., 2012). Among the approaches, surfactant-alternating-gas is the preferred method (Matthews, 1989; Heller, 1994), due to its enhanced gas injectivity, and its capability of reducing the risk of corrosion in surface facilities and piping (Matthews, 1989; Schramm, 1994). However, SAG processes often suffer from poor liquid injectivity (Kuehne et al., 1990; Martinsen and Vassenden, 1999). To prevent the injection well from fracturing, it is

* Corresponding author. College of Mechanics and Materials, Hohai University, Nanjing, 210098, Jiangsu, China.
E-mail address: jiakungong@hhu.edu.cn (J.-K. Gong).

https://doi.org/10.1016/j.petsci.2023.10.010
1995-8226/© 2023 The Authors. Publishing services by Elsevier B.V. on behalf of KeAi Communications Co. Ltd. This is an open access article under the CC BY-NC-ND license (http://creativecommons.org/licenses/by-nc-nd/4.0/).

necessary to decrease the rate at which liquid is injected.

The injectivity of liquid in a SAG foam process is dominated by the near-well flow behaviour. Our previous work (Gong et al., 2019, 2020a, 2020b, 2020c) shows that a collapsed-foam area emerges in the vicinity of the injection face during gas injection and slowly propagates downstream. In this region, foam either fully collapses or significantly weakens, resulting in a small amount of trapped gas. During the following liquid-injection period, liquid first rapidly infiltrates the collapsed-foam area, re-trapping some of the gas in place and sweeping nearly the entire cross section, and then forms fingers as it flows through the trapped foam in the downstream area. Afterwards, a bank emerges in the foam area outside of the collapsed foam region. This bank is characterized by gas within the fingers dissolving into unsaturated liquid or being displaced, resulting in a significant increase in mobility (Gong et al., 2020a). The collapsed-foam region formed during gas injection greatly improves subsequent liquid injectivity, since liquid mobility in this region during the liquid-injection period is much greater than that further from the injection well.

Cores with similar permeability were used in those studies. Underground reservoirs are heterogeneous, often layered (Lake et al., 2014), which could make the near-well flow behaviour more complex. Current studies of the effect of permeability on foam focus mainly on two aspects. One is the effect of formation permeability on the mobility of foam at steady state. Foam is found to be stronger in higher-permeability formations (Lee et al., 1991; Kapetas et al., 2017). Another aspect of the effect of permeability on foam is foam flow behaviour in heterogeneous reservoirs. Studies have been conducted in layered porous media with and without crossflow between layers. When crossflow is allowed, foam propagates at similar rates in each layer; foam fronts move more rapidly through the lower-permeability layer, when capillary communication between layers is prohibited (Yaghoobi and Heller, 1996; Rossen and Lu, 1997; Bertin et al., 1998; Ding et al., 2022).

Implicit-texture (IT) models (Cheng et al., 2000; Computer Modeling Group Ltd, 2006) are commonly utilized for numerical simulation of foam transport in porous media. In these models, the impact of foam on gas mobility is characterised by a mobility-reduction factor that is dependent on surfactant concentration, water and oil saturations, capillary number and other related variables. Farajzadeh et al. (2015) found that all parameters in the IT foam models depend on permeability. Specifically, as permeability increases, the values of *fmdry* (which indicates the water saturation at the limiting capillary pressure) and *epdry* (which governs the suddenness of foam coalescence) decrease.

Thus, previous studies of the effect of permeability on foam flow have focused on steady-state foam properties and the in-depth foam-displacement process. The effect of permeability on flow behaviour at the injection face during foam injection is not well documented.

In this study, we first perform coreflood experiments of SAG foam injection in sandstone cores with permeabilities ranging from 16 to 2300 mD. Our analysis investigates how permeability impacts gas injectivity during foam-based gas injection, liquid injectivity during foam-based liquid injection, and liquid injectivity during liquid injection following a period of gas injection. Furthermore, investigations are conducted on the impact of superficial velocity during gas and liquid injection. Subsequently, we utilize a radial model to extrapolate the experimental results regarding the spread of banks from the injection well and analyze the potential implications for practical implementation in the field. The bank-propagation model (Gong et al., 2019, 2020c) is updated to incorporate the bank properties that are dependent on superficial velocity, which are determined for each permeability through coreflood experiments.

2. Materials and methods

2.1. Experimental materials and apparatus

A serious of coreflood experiments were conducted in sandstone core samples with various permeabilities: Fontainbleu (16 mD), Berea (150 mD) and Bentheimer (2300 mD). The porosities of the cores are 0.06, 0.21 and 0.23, respectively. The cores are all 17 cm long, with a diameter of 3.8 cm. The tests are performed under a 40-bar back pressure and at a temperature of 90 °C. A surfactant solution is created by combining alpha olefin sulfonate ($AOS_{C14\text{-}16}$) surfactant and synthetic brine with a salinity of 3 wt% to achieve a concentration of 0.5 wt%. The synthetic brine is composed of five salts, namely potassium chloride, calcium chloride, sodium sulphate, magnesium chloride, and sodium chloride. The experimental apparatus is schematically shown in Fig. 1. The cores are positioned in a vertical orientation to reduce the effect of gravity override, and subjected to a temperature of 90 °C inside an oven during the experiments. Nitrogen, along with the surfactant solution, is introduced into the core through a mass-flow controller and a Quizix pump, with injection taking place from the bottom. To sustain a back-pressure of 40 bar, the outlet is linked with a back-pressure regulator. To monitor both the absolute pressures at different positions along the core and the pressure drops across its sections, six pressure transducers are utilized. In this study, we focus on the three middle sections (Sections 2–4), which are each 4.2 cm in length, in order to avoid the entrance and capillary-end effects (Apaydin and Kovscek, 2001).

2.2. Experimental methods

Three groups of experiments were performed: (1) Effect of permeability on the injectivity of gas in a SAG foam process. A large amount of gas is injected after steady-state nitrogen foam injection. (2) Effect of permeability on the injectivity of liquid directly after foam. Liquid is injected directly following steady-state foam. (3) Effect of permeability on the injectivity of liquid in a SAG foam process. After achieving a steady-state foam, liquid is injected after an equivalent quantity of gas injection. The details of the experiments are listed in Table 1.

3. Experimental results

In this section, we first present the experimental results, and then discuss the effect of permeability on the near-wellbore flow behaviour in a SAG foam process.

3.1. Effect of permeability on gas injectivity in a SAG process

To investigate how formation permeability impacts gas injectivity in a SAG foam process, gas is injected continuously for an extended period at a consistent superficial velocity of 6 ft/day (2.12×10^{-5} m/s) following steady-state foam (injected gas volume fraction, or "quality" $f_g = 0.95$). As shown in Fig. 2, regardless of the formation permeability, a similar flow pattern is observed. The pressure gradient first declines to a plateau, indicating foam weakening. The sectional pressure gradients are comparable in each case, i.e. about 3 bar/m for the high-permeability core (Bentheimer core), about 10 bar/m for the medium-permeability core (Berea core), about 20 bar/m for the low-permeability core (Fontainebleau core). The sectional pressure gradients then slowly decrease to a very low value, which happens in a wave pattern from Section 2 to Section 4. This implies that the bank of collapsed foam spreads slowly from the entrance towards the outflow of the core. Within this area, foam fully collapses or loses much of its strength,

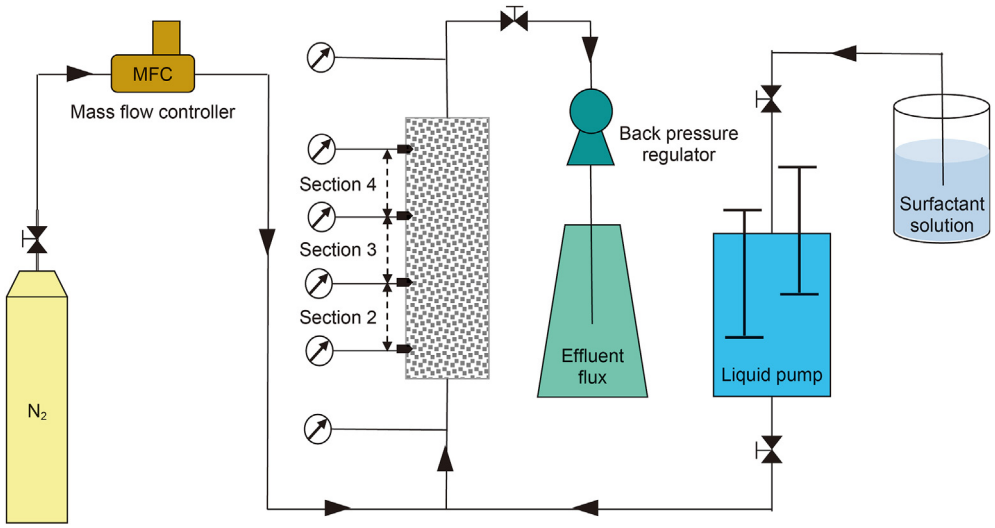

Fig. 1. Schematic of experimental apparatus.

Table 1
Summary of coreflood experiments.

No.	Permeability, mD	Foam injection		Gas injection		Liquid injection	
		Total superficial velocity, ft/day*	Quality**	Superficial velocity, ft/day	Injection volume, PV	Superficial velocity, ft/day*	Injection volume, PV
P1-1	2300	2	0.95	–	–	2	15
P1-2		2	0.95	3	175	–	–
P1-3		2	0.95	6	193	–	–
P1-4		2	0.95	9	198	–	–
P1-5		2	0.95	6	10	2	8
P1-6		2	0.95	6	40	2	12
P1-7		2	0.95	6	80	2	9
P1-8		2	0.95	6	80	20	20
P1-9		2	0.95	6	80	80	52
P1-10		2	0.95	6	80	200	115
P2-1	150	2	0.95	–	–	2	10
P2-2		2	0.95	3	360	–	–
P2-3		2	0.95	6	242	–	–
P2-4		2	0.95	9	320	–	–
P2-5		2	0.95	6	10	2	17
P2-6		2	0.95	6	50	2	17
P2-7		2	0.95	6	150	2	17
P2-8		2	0.95	6	150	20	34
P2-9		2	0.95	6	150	80	69
P2-10		2	0.95	6	150	200	68
P3-1	16	2	0.95	–	–	2	69
P3-2		2	0.95	3	291	–	–
P3-3		2	0.95	6	202	–	–
P3-4		2	0.95	9	342	–	–
P3-5		2	0.95	6	10	2	59
P3-6		2	0.95	6	40	2	50
P3-7		2	0.95	6	60	2	64
P3-8		2	0.95	6	80	2	53
P3-9		2	0.95	6	60	20	141
P3-10		2	0.95	6	60	40	65

Note: *1 ft/day = 0.305 m/day; ** injected gas volume fraction at core back-pressure.

resulting in only a small amount of trapped gas remaining. The formation and spread of the so called collapsed-foam bank are the result of a complicated combination of processes such as evaporation, gas dissolution, viscous effects, and capillary action (Gong et al., 2020a). The collapsed-foam front propagates somewhat faster in the high-permeability core sample. The pressure gradient in Section 4 reaches its ultimate value, indicating that the collapsed-foam front has reached the final portion of Section 4. This occurs after roughly 145 PV of gas injection for the core with high permeability, and approximately 170 PV of gas injection for the core with the lowest permeability.

We then examine how the gas superficial velocity impacts the flow behaviour in the gas-injection period. The pressure gradients in Section 4 are taken for comparison here for illustration. According to the data illustrated in Fig. 3, it can be observed that the collapsed-foam region exhibits comparable dimensionless propagation velocities for gas injection rates of 3 and 6 ft/day, both in the case of low and high permeabilities. However, when the gas

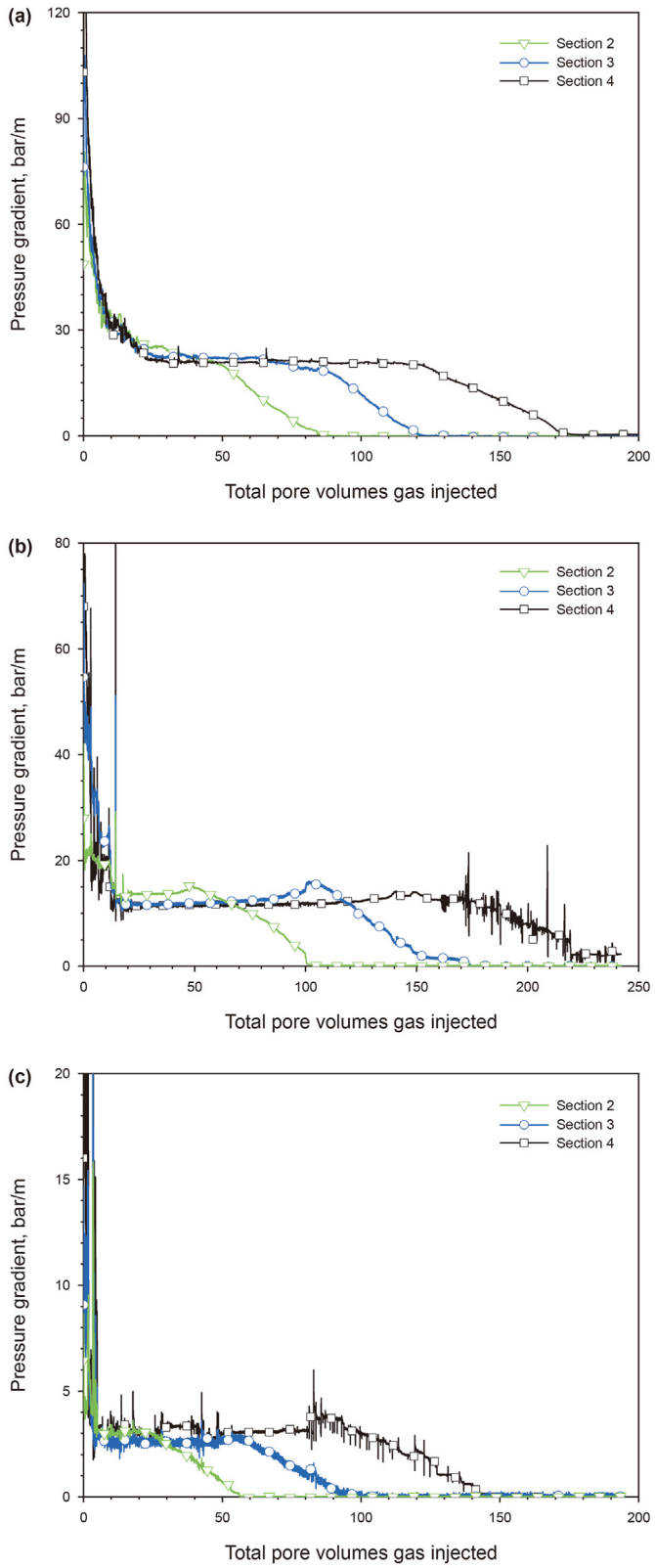

Fig. 2. Pressure gradients during gas injection at 6 ft/day following 0.95-quality foam. (**a**) Fontainebleau; (**b**) Berea; (**c**) Bentheimer.

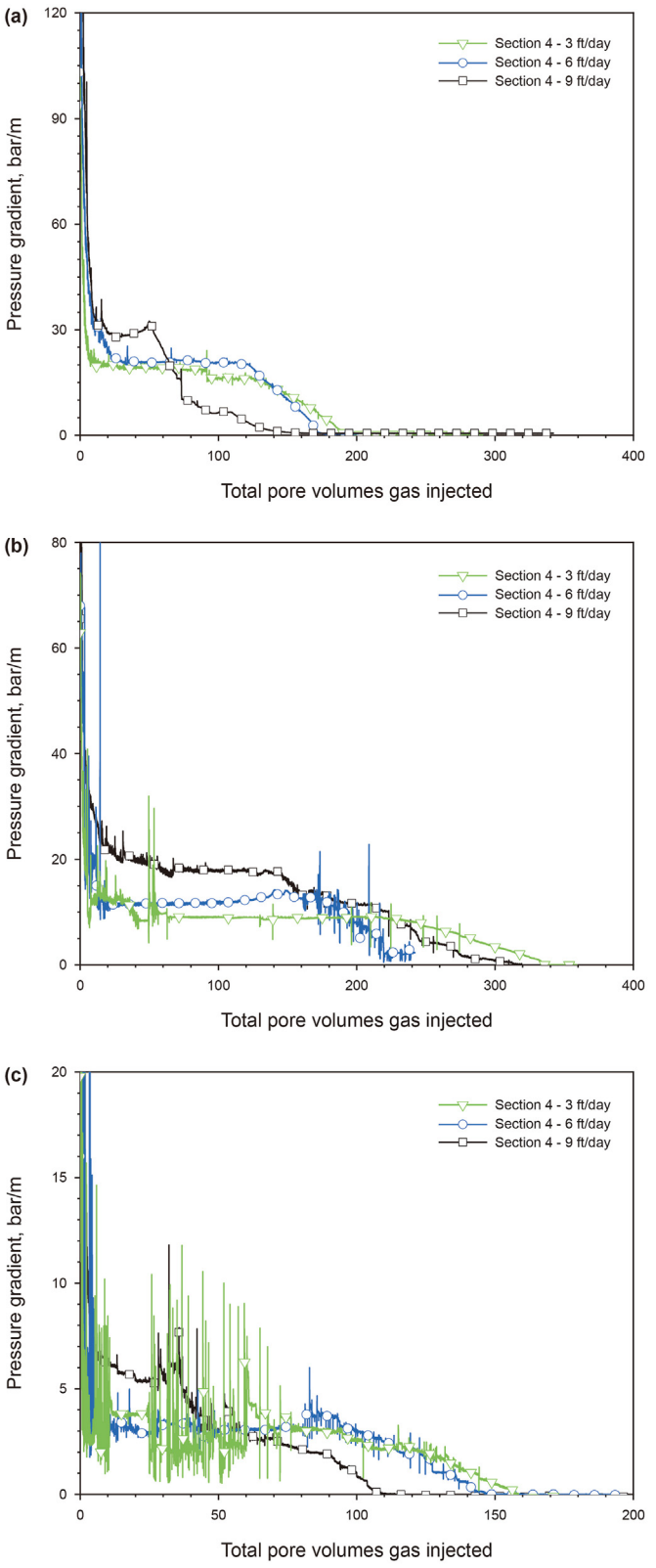

Fig. 3. Pressure gradients during gas injection at various superficial velocities. (**a**) Fontainebleau; (**b**) Berea; (**c**) Bentheimer.

injection rate is increased to 9 ft/day (as shown in Fig. 3(a) and (c)), the collapsed-foam region propagates approximately 1.3 times faster. In contrast, for the medium permeability, the dimensionless velocities of the collapsed-foam region exhibit similarities for gas injection rates of 3 and 9 ft/day. However, when gas is injected at a rate of 6 ft/day, the collapsed-foam region propagates approximately 1.4 times faster (as depicted in Fig. 3(b)). For modelling purposes, we conclude that the velocity at which the collapsed-foam front propagates is not greatly influenced by the superficial velocity of gas injection.

As proposed in our previous work (Gong et al., 2020b), the total mobility and the dimensionless propagation velocity can be applied to characterize the characteristics of the banks. To determine the total mobility ($u_t/\nabla p$) of a bank, Darcy's law is applied by approximating foam flow as single-phase flow, whereby the total superficial velocity (u_t) is divided by the pressure gradient (∇p). The dimensionless propagation velocity of the front of a bank is determined in a way as follows: suppose the collapsed-foam front arrives at a position 2/3 of the length of the core after about 100 PV of gas injection (total pore volume of the core), which corresponds to about 150 LPV (local pore volume) from the front position back to the inlet, then the dimensionless propagation velocity then can be calculated as 1/150. As discussed above, during the period of gas injection, the core is occupied by the collapsed-foam region and the foam region, as demonstrated by the experimental results. Table 2 provides a listing of the bank properties calculated based on the experimental data.

As listed in Table 2, for each permeability, the superficial velocity has little impact on the total mobility and the dimensionless velocity at which the collapsed-foam bank propagates. The dimensionless velocity is somewhat affected by permeability; however, no consistent trend is observed. The dimensionless velocities for various formation permeabilities are of the same magnitude. Given the relatively small difference in dimensionless propagation velocity and the large differences in permeability, we conclude that the formation permeability has little effect on the dimensionless propagation velocity of the front of collapsed-foam region. In contrast, the total mobility of the collapsed-foam bank is strongly impacted by permeability: for both the foam and collapsed-foam banks, the greater the permeability, the greater the reduction in total mobility. In other words, foam is stronger in porous media with higher permeability (Lee et al., 1991; Kapetas et al., 2017).

3.2. Effect of permeability on liquid injectivity in a SAG process

In this present part, liquid injection immediately after full-strength foam and liquid injection after a time of gas injection in a SAG foam process are both examined to see how their injectivity is affected by permeability.

Firstly, we analyze the injectivity of liquid in liquid injection after foam, which represents the worst liquid injectivity. Fig. 4 presents the change in pressure gradient observed during the injection of liquid after foam with quality of 0.95. As shown in Fig. 4, the liquid shows a similar trend in flow behaviour, regardless the permeability. Liquid first flows in with a relatively low mobility and penetrates foam. Then the pressure gradient reaches a plateau (which we call the forced-imbibition bank). As more liquid is injected, the pressure gradient declines again as a wave (which we call the gas-dissolution bank) from the inlet towards downstream. This decline can be explained by gas dissolution and liquid fingering (Gong et al., 2020b). At first, liquid sweeps the entire cross-sectional area of the core. As more liquid flows through, trapped gas starts to dissolve into the flowing unsaturated liquid, which leads to the formation of a liquid finger. The liquid finger takes almost all liquid flow, and grows downstream as more liquid is injected. It also slowly grows radially outward by dissolving gas surrounding it (Gong et al., 2020b). Permeability affects the value at which the pressure gradient plateaus: about 20 bar/m for the high-permeability core, while it is about 80 bar/m for the low-permeability core. The plateau values in the sectional pressure gradients differ in various sections: about 40 bar/m for Section 2, 60 bar/m for Section 3 and 80 bar/m for Section 4, averaging about 60 bar/m for the medium-permeability core. The gas-dissolution bank propagates faster in the higher-permeability cores. For Section 4, the decline in pressure gradient happens from 6 to 8 PV liquid injection in the high-permeability core, from 3 to 7 PV liquid injection in the medium-permeability core, and between 32 and 45 PV liquid injection in the low-permeability core.

The impact of a time of gas injection on the following liquid injectivity in cores with varying permeabilities is illustrated in Fig. 5. In the case of Section 2 of the high-permeability core, as depicted in Fig. 5(e), the value at which the pressure gradient plateaus is about 15 bar/m during injection of liquid following approximately 10 PV of gas injection, slightly lower compared to the case in which liquid is injected immediately after foam (Fig. 4(c)). The value at which the pressure gradient plateaus is less if more gas was injected previously: if 40 PV of gas is injected beforehand, the plateau value is 5 bar/m, whereas if 80 PV of gas is injected, the plateau value is less than 1 bar/m (Fig. 5(e)). The collapsed-foam bank reaches and propagates through Section 2 as more gas is injected, which improves liquid injectivity greatly. On the contrary, in Section 4, the plateau values are nearly unaffected by these amounts of gas injected (Fig. 5(f)); the collapsed-foam region has not yet arrived in Section 4. In both Sections 2 and 4, the plateau lasts longer with a larger amount of gas injected beforehand. Injecting more gas results in an increase in the amount of gas present in the larger collapsed-foam region, which in turn requires a greater amount of liquid to dissolve the gas. As a result, the plateau duration is extended.

In the medium- and low-permeability cores (Fig. 5(a)–(d)), the pressure gradient alteration when injecting liquid after various amounts of gas follows a similar trend to the high-permeability core. In Section 2, as more gas is injected, the plateau value decreases, due to the propagation of the bank in which foam collapses or greatly weakens through that section. In contrast, the plateau value in Section 4 is nearly unaffected by the gas injection in the

Table 2
Comparison of bank properties during gas injection period.

Bank	Superficial velocity, ft/day	Dimensionless velocity			Total mobility, $m^2/(Pa\ s)$		
		Bentheimer	Berea	Fontainebleau	Bentheimer	Berea	Fontainebleau
Collapsed-foam	3	5.4×10^{-3}	2.8×10^{-3}	4.5×10^{-3}	8.2×10^{-9}	4.6×10^{-9}	4.2×10^{-10}
	6	6.2×10^{-3}	1.8×10^{-3}	5.0×10^{-3}	9.8×10^{-9}	3.5×10^{-9}	6.0×10^{-10}
	9	7.8×10^{-3}	2.3×10^{-3}	5.4×10^{-3}	9.8×10^{-9}	4.2×10^{-9}	6.3×10^{-10}
Foam	3	Initial state	Initial state	Initial state	2.5×10^{-11}	1.5×10^{-11}	5.3×10^{-12}
	6	Initial state	Initial state	Initial state	6.0×10^{-11}	2.3×10^{-11}	1.0×10^{-11}
	9	Initial state	Initial state	Initial state	1.1×10^{-10}	2.3×10^{-11}	1.1×10^{-11}

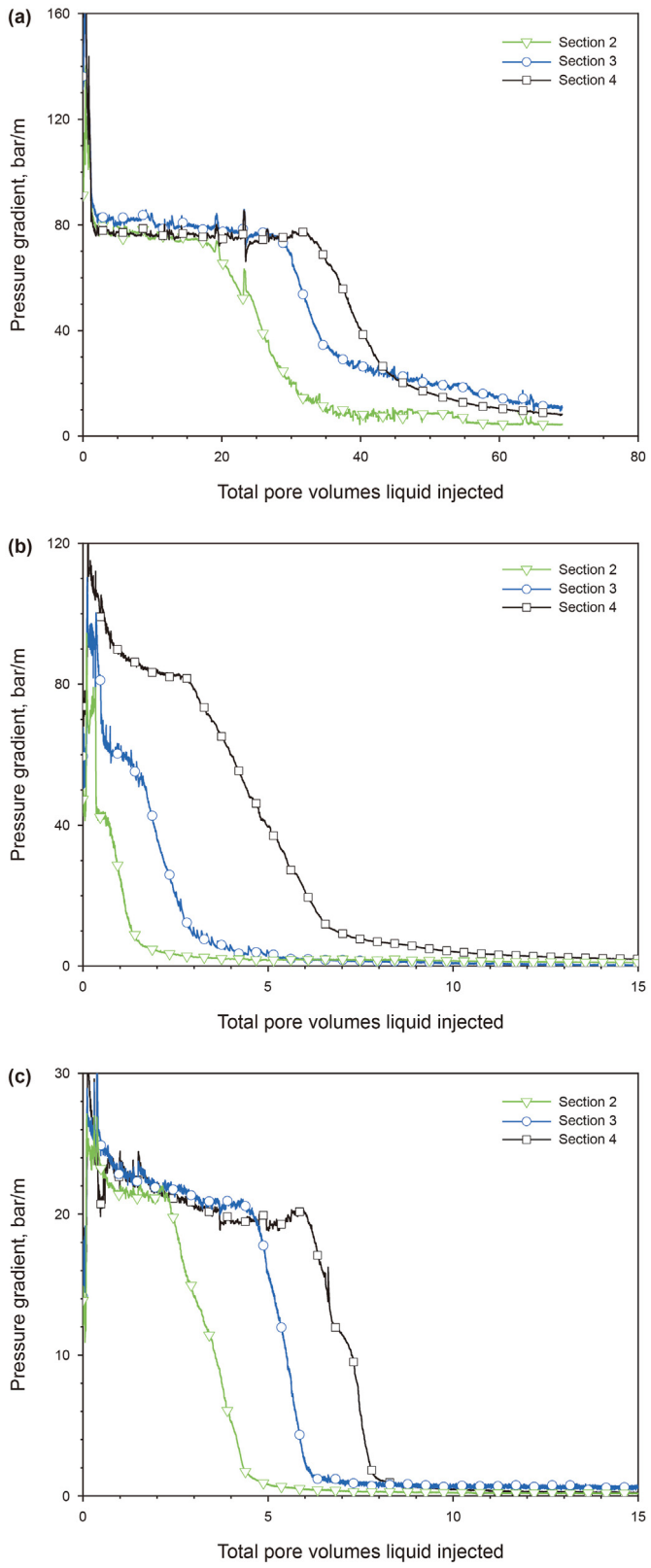

Fig. 4. Injection of liquid after foam (f_g = 0.95). (**a**) Fontainebleau; (**b**) Berea; (**c**) Bentheimer.

previous period. However, the effect of gas-injection quantity on the duration of the plateau during liquid injection in the low-permeability core is not as obvious as that in the high-permeability core.

A series of experiments are performed to investigate how the superficial velocity impacts the flow behaviour in the liquid-injection period. Due to the limitation of maximum pressure of our apparatus, for the low-permeability core, we could examine the liquid injectivity only at superficial velocities up to 40 ft/day. Our interest lies in how the superficial velocity affects liquid flow in the region in which foam collapses or greatly weakens as well as the foam region that extends beyond it. Therefore, for each permeability, gas is injected after 0.95-quality foam in order to create a collapsed-foam region in the core. However, various amounts of gas are injected for different permeabilities, as the collapsed-foam front propagates at varying velocities: 60 PV for Fontainebleau core sample (low-permeability core), 150 PV for Berea core (medium-permeability core), and 80 PV for the Bentheimer core sample (high-permeability core). In the experiments with Bentheimer core, for example, we first inject 80 PV of gas after foam; the front of the collapsed-foam bank enters Section 3 of the core.

Then we investigate how the flow behaviour changes in both the collapsed-foam region (Section 2) and the foam region beyond it (Section 4) as a result of varying liquid superficial velocity. As shown in Fig. 6, similar flow behaviour is observed at all the permeabilities examined. There is a comparable pattern in the pressure gradient when injecting liquid at low and high superficial velocities. However, at higher superficial velocity, the plateau becomes less obvious, and the pressure gradient requires a significantly longer period to reach the final stage of reduction. The liquid flow behaviour in both the collapsed-foam region (Section 2) and the foam region (Section 4) are strongly affected by liquid superficial velocity. In the high-permeability core, for example, when liquid flows into the collapsed-foam region, the pressure gradient increases from about 0.5 bar/m to about 16 bar/m (Fig. 6(e)), about 32 times, while the injection velocity increases 100 times: a shear-thinning flow behaviour is observed. This indicates that there are still some foam bubbles trapped in the collapsed-foam area, although the foam is greatly weakened. The shear-thinning flow behaviour during liquid injection is more striking in the area where foam is not collapsed or greatly weakened (Fig. 6(f)). When the velocity of liquid injection rises from 2 to 200 ft/day (100 times), the plateau value in pressure gradient increases by only about 2 times (from about 12 bar/m to about 24 bar/m), while the final value in pressure gradient increases from about 1 to 8 bar/m, about 8 times.

As discussed above, when liquid is injected subsequent to a time of gas injection after foam, the vicinity of the injection well can be occupied by several banks: the collapsed-foam bank, the forced-imbibition bank, the gas-dissolution bank and the foam bank. The total mobilities and the dimensionless propagation velocities of the banks at various liquid superficial velocities are listed in Table 3. At relatively low liquid injection velocity (2 ft/day (0.61 m/day) and 20 ft/day), the liquid fills the collapsed-foam region quicker with a reduced total mobility in the higher-permeability formation. The same trend applies to the forced-imbibition bank and the gas-dissolution bank: the banks propagate faster and with a greater reduction in total mobility in the higher-permeability formation. When liquid is injected at a high velocity, however, we cannot observe the complete trend of bank properties with permeability, because the pressure gradient which occurs in the low-permeability core (Fontainebleau) at 200 ft/day (61 m/day) is beyond the limitation of our setup.

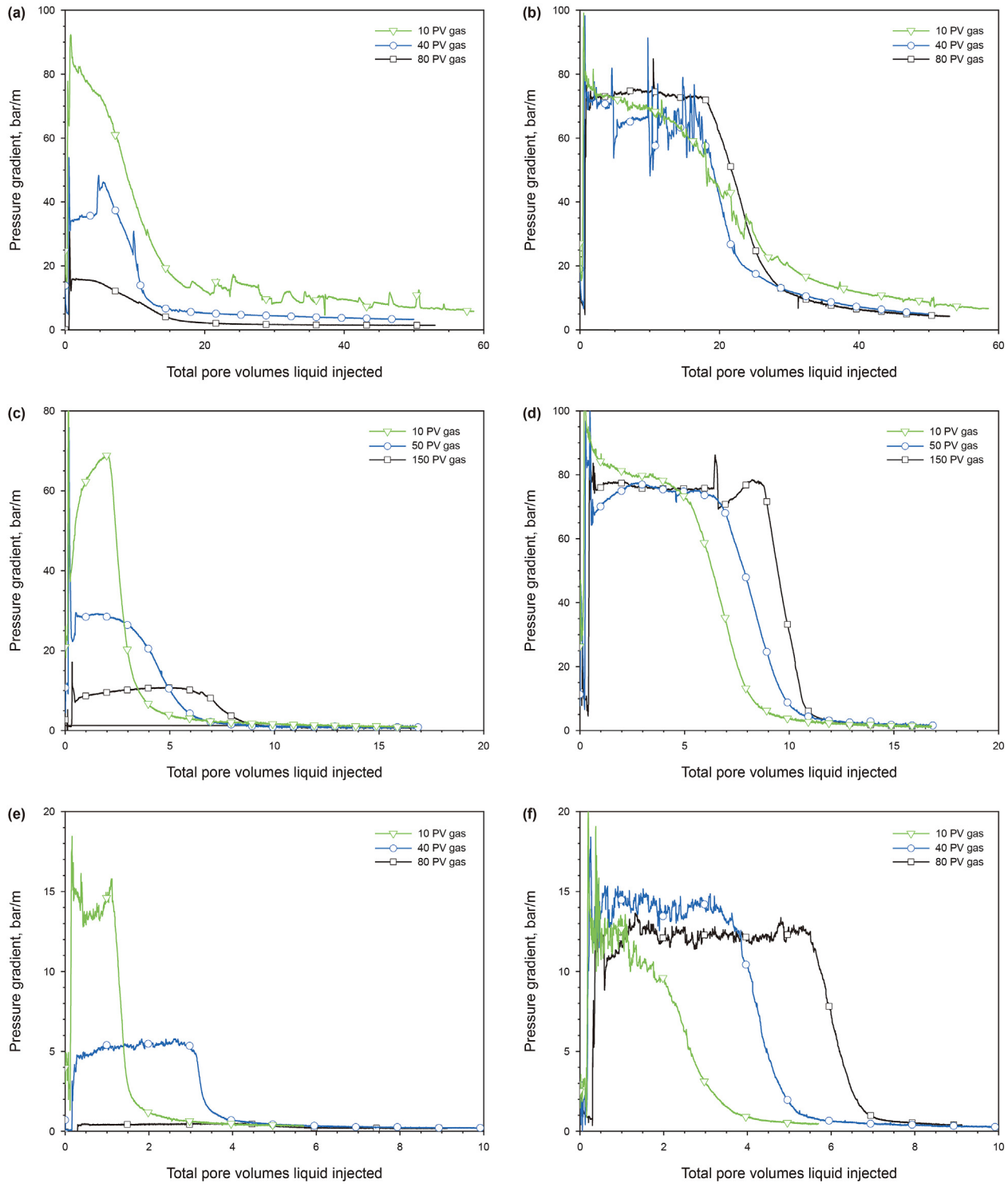

Fig. 5. Liquid injection following various amount of gas injection after 0.95-quality foam in various-permeability formation. (**a**) Section 2, Fontainebleau; (**b**) Section 4, Fontainebleau; (**c**) Section 2, Berea; (**d**) Section 4, Berea; (**e**) Section 2, Bentheimer; (**f**) Section 4, Bentheimer.

4. Implications for field application

Our earlier work proposes that the injectivity of liquid in a SAG foam process is dominated by the spread of multiple banks and their associated properties (Fig. 7). Nevertheless, traditional foam models based on Peaceman equation are inadequate in representing the bank propagation occurring in a SAG foam process, especially the impact of gas injection on subsequent liquid injectivity. This leads to an incorrect estimation of the injectivities of gas and liquid in a SAG foam process (Gong et al., 2019). To address this limitation, a bank-propagation model derived from the experimental findings was proposed to capture the influence of the bank propagation on the evolution of liquid injectivity in a SAG foam process (Gong et al., 2019). In this section, we utilize the bank-

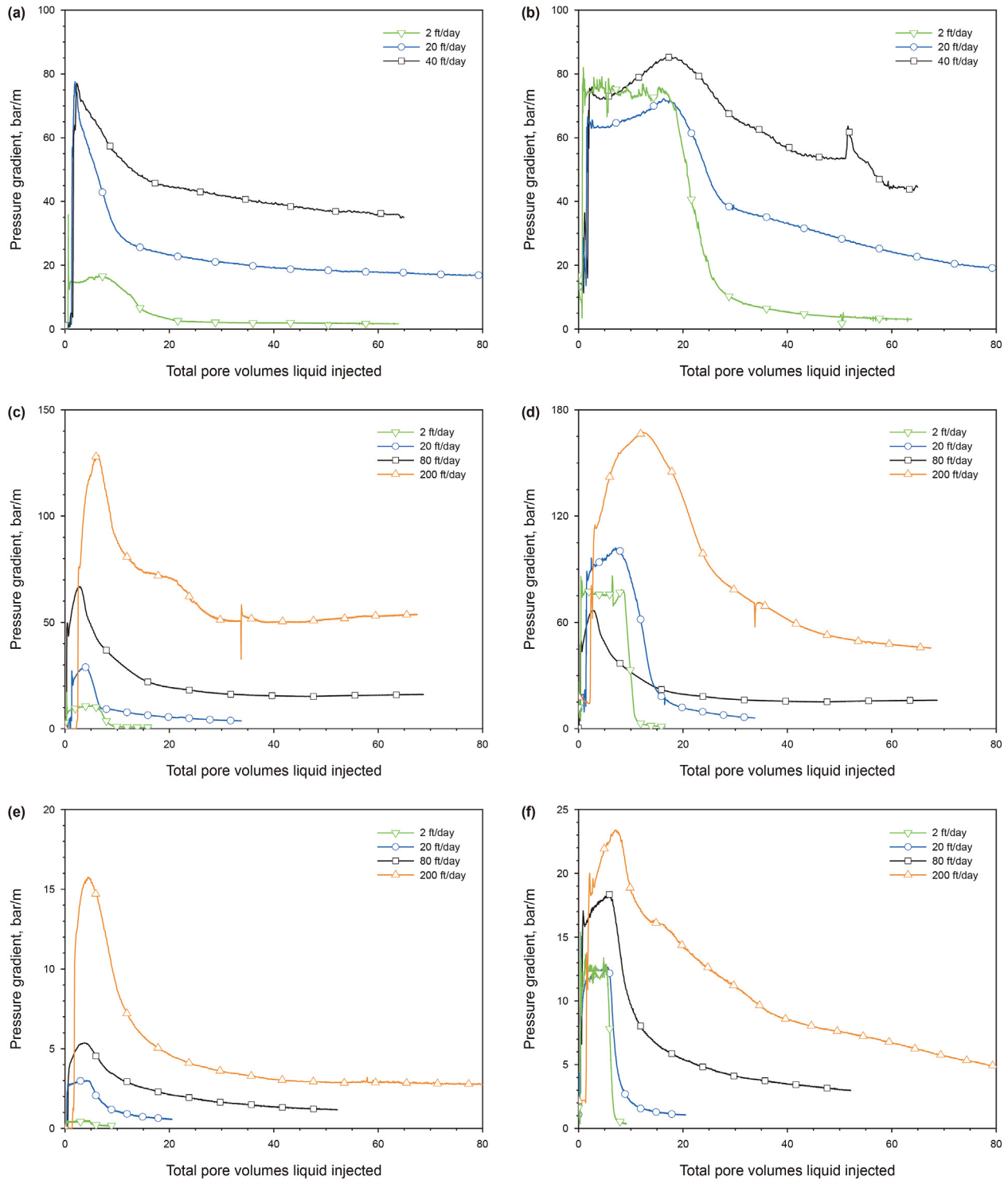

Fig. 6. Pressure gradients in the collapsed-foam region (Section 2) and foam region (Section 4) during liquid injection at varying superficial velocities following a period of gas injection after 0.95-quality foam. (**a**) Section 2, Fontainebleau. (**b**) Section 4, Fontainebleau. (**c**) Section 2, Berea. (**d**) Section 4, Berea. (**e**) Section 2, Bentheimer. (**f**) Section 4, Bentheimer.

propagation model to upscale the experimental results discussed earlier. Our objective is to explore the influence of permeability on the injectivity of liquid at the field scale. A comparative analysis is conducted to assess the liquid injectivity estimates obtained from the bank-propagation model and the conventional foam simulators.

In the bank-propagation model, it is assumed that the behaviour observed at the core scale directly scales up to the field scale. The banks are assumed to spread radially around the injection well with the dimensionless velocities derived from coreflood experiments. The radius of the wellbore (r_w) is fixed at 0.1 m, and the outer radius (r_e) is fixed at 20 m, which is corresponding to the Peaceman-

Table 3
Comparison of bank properties during liquid injection period.

Bank	Superficial velocity, ft/day	Dimensionless velocity			Total mobility, $m^2/(Pa\ s)$		
		Bentheimer	Berea	Fontainebleau	Bentheimer	Berea	Fontainebleau
Collapsed-foam	2	0.83	0.76	0.39	2.6×10^{-10}	1.4×10^{-10}	2.3×10^{-11}
	20	0.86	0.72	0.18	8.7×10^{-10}	1.8×10^{-10}	3.5×10^{-11}
	40	–	–	0.14	–	–	2.5×10^{-11}
	80	0.28	0.81	–	1.8×10^{-9}	1.9×10^{-10}	–
	200	0.65	0.65	–	9.4×10^{-10}	2.7×10^{-10}	–
Forced-imbibition	2	9.36	2.5	2.72	5.5×10^{-12}	8.6×10^{-13}	1.3×10^{-12}
	20	7.26	2.1	1.34	5.3×10^{-11}	6.4×10^{-12}	1.0×10^{-11}
	40	–	–	1.18	–	–	1.7×10^{-11}
	80	1.45	1.79	–	1.4×10^{-10}	2.4×10^{-11}	–
	200	1.09	1.67	–	2.8×10^{-10}	4.7×10^{-11}	–
Gas-dissolution	2	0.13	0.08	0.02	3.3×10^{-10}	5.0×10^{-11}	2.2×10^{-11}
	20	0.1	0.07	0.03	7.7×10^{-10}	1.0×10^{-10}	3.9×10^{-11}
	40	–	–	0.03	–	–	4.0×10^{-11}
	80	0.06	0.04	–	1.5×10^{-9}	1.6×10^{-10}	–
	200	0.03	0.04	–	2.2×10^{-9}	1.8×10^{-10}	–
Foam	2	Initial	Initial	Initial	6.0×10^{-11}	2.3×10^{-11}	1.0×10^{-11}
	20	Initial	Initial	Initial	6.0×10^{-11}	2.3×10^{-11}	1.0×10^{-11}
	40	–	–	Initial	–	–	1.0×10^{-11}
	80	Initial	Initial	–	6.0×10^{-11}	2.3×10^{-11}	–
	200	Initial	Initial	–	6.0×10^{-11}	2.3×10^{-11}	–

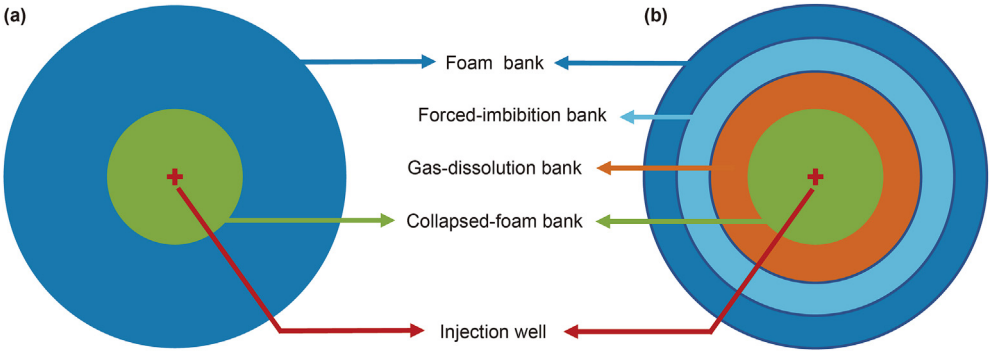

Fig. 7. Banks observed in SAG-foam coreflood experiments (Gong et al., 2020c). (**a**) Banks during the gas-injection period; (**b**) Banks during the liquid-injection period.

defined equivalent radius (Peaceman, 1978) for a grid block measuring 100 m × 100 m. Assuming full saturation with water initially, the area of focus is flushed by foam at a dimensionless speed of one. The total pressure difference between the wellbore and the outer radius is determined by summing up the pressure differences across varying banks. During the period of gas injection, the pressure differences across the collapsed-foam bank, the foam bank and the water bank preceding the foam bank for a specific time frame are taken into account. Throughout the liquid injection phase, the overall pressure difference is calculated by summing up the pressure differences across the collapsed-foam bank, the gas-dissolution bank, the forced-imbibition bank, and the foam bank. The application of Darcy's law to radial flow enables the calculation of the pressure difference for every bank.

As discussed above, the gas superficial velocity has little impact on the bank properties of formations with varying permeability during gas injection. Thus, when gas is injected, our bank-propagation model assumes each bank propagates with a uniform dimensionless velocity and a consistent total mobility. In the phase of liquid injection, uniform bank properties are assumed when liquid flows in the collapsed-foam area. In contrast, for all the permeabilities examined, power-law equations can be applied to describe the relationships between the superficial velocities (v_s) and the dimensionless propagation velocities and the total mobilities of the gas-dissolution bank and the forced-imbibition bank. The details of the bank properties assumed in the bank-propagation model are listed in Table 4. The specifics of the model are described thoroughly in our earlier study (Gong et al., 2019, 2020c).

For comparison purpose, we utilize the Peaceman equation and the implicit-texture (IT) foam model algorithm (Cheng et al., 2000) as the conventional method, to compute the increase in well pressure caused by the injection of gas and liquid in a SAG foam process. The model portrays the impact of foam on gas mobility through a mobility-reduction factor, which is dependent on multiple factors, such as water saturation, surfactant concentration, etc. The gas mobility without foam at the given saturation is multiplied by this factor to represent gas mobility with foam. The following assumptions are made in this model: the formation has a consistent height, and the injection well penetrates the entire interval; rock, water and gas are considered to be incompressible; there is no oil present in the grid block; the grid block is entirely saturated with water when gas injection commences; water saturation in the grid block remains uniform throughout; the impact of gravity is neglected; neither viscous fingering nor dispersion are taken into account. The viscosities of water and gas are set to 3.2×10^{-4} and 2.0×10^{-5} Pa s, respectively. The input parameters of the foam simulator for the formations examined here are listed in Tables 5 and 6. The parameter *fmdry* is defined as the water saturation at the transition from low-quality foam regime to high-quality regime, while *epdry* controls the abruptness of this transition. The

Table 4
Bank properties for varying injection phase.

Period	Bank	Dimensionless velocity			Total mobility, $m^2/(Pa\ s)$		
		Bentheimer	Berea	Fontainebleau	Bentheimer	Berea	Fontainebleau
Gas injection	Collapsed-foam	6.2×10^{-3}	1.8×10^{-3}	5.0×10^{-3}	9.8×10^{-9}	3.5×10^{-9}	5.9×10^{-10}
	Foam	1	1	1	5.9×10^{-11}	2.3×10^{-11}	9.3×10^{-12}
	Water	Initial state	Initial state	Initial state	2.3×10^{-9}	1.5×10^{-10}	1.5×10^{-11}
Liquid injection	Collapsed-foam	0.56	0.76	0.24	9.5×10^{-10}	1.4×10^{-10}	2.6×10^{-11}
	Forced-imbibition	$17.3v_s^{-0.5}$	$2.7v_s^{-0.09}$	$3.3v_s^{-0.29}$	$3 \times 10^{-12}v_s^{0.86}$	$5 \times 10^{-13}v_s^{0.88}$	$7 \times 10^{-13}v_s^{0.85}$
	Gas-dissolution	$0.2v_s^{-0.31}$	$0.1v_s^{-0.18}$	$2 \times 10^{-2}v_s^{-0.06}$	$2 \times 10^{-10}v_s^{0.41}$	$4 \times 10^{-11}v_s^{0.29}$	$2 \times 10^{-11}v_s^{0.21}$
	Foam	Initial state	Initial state	Initial state	5.9×10^{-11}	2.3×10^{-11}	9.3×10^{-12}

Table 5
Relative-permeability parameters of cores.

Parameter	Value		
	Bentheimer	Berea	Fontainebleau
n_g	0.70	1.22	1.54
n_w	2.86	5.25	2.20
k^o_{rg}	0.59	0.47	0.2
k^o_{rw}	0.39	0.14	0.14
S_{gr}	0.20	0.25	0.18
S_{wr}	0.25	0.20	0.30

Table 6
Foam parameters extracted from foam-quality scan.

Parameter	Value		
	Bentheimer	Berea	Fontainebleau
fmdry	0.27	0.31	0.33
epdry	4.9×10^3	6.5×10^3	1.5×10^4
fmmob	8.4×10^3	6.8×10^3	4.0×10^3
epcap	2.5	2.1	1.5
fmcap	6.7×10^{-4}	5.6×10^{-5}	4.0×10^{-6}

parameter *fmmob* is the reference gas-mobility-reduction factor, which corresponds to the maximum-attainable mobility reduction. The parameters *epcap* and *fmcap* represent the non-Newtonian behavior in the low-quality regime and the reference capillary number, respectively. The foam parameters are obtained by fitting the foam-quality scan data at a single superficial velocity. Boejie and Rossen's foam-model parameter-fitting method (Boeije and Rossen, 2015) is utilized for an initial estimation of the foam parameters. The fit is then further refined using Farajzadeh's least-squares optimization program (Farajzadeh et al., 2015). Additional information about the model is available in our previous work (Gong et al., 2019, 2020c). As expected, the maximum apparent viscosity is much greater in the higher-permeability cores: 1.3, 0.4 and 0.06 Pa s in Bentheimer, Berea and Fountainebleau, respectively.

The pressure drop in this research is expressed as a dimensionless value, calculated by dividing the difference in pressure between the wellbore radius (r_w) and the outer radius(r_e) by the pressure difference resulting from injecting water at the volumetric rate $Q_0 = 4.5 \times 10^{-4}$ $m^3/(s\ m)$ ($39\ m^3/(day\ m)$) into an area full of water. The pore volume of a 100 m × 100 m × 1 m grid block (GPV) is used to express the dimensionless time and the sizes of gas and liquid slugs.

Fig. 8 compares the injectivity of liquid following injection of various amounts of gas, estimated by the bank-propagation model and the conventional simulation algorithm. Regardless of the formation permeability, the conventional simulation algorithm cannot reflect the impact of previous gas injection phase on the following liquid injectivity. The more gas is injected, the more inaccurate the liquid injectivity estimated from the Peaceman equation becomes. For the high-permeability formation (Fig. 8(c)), the conventional simulation algorithm underestimates liquid injectivity (overestimates the dimensionless pressure drop) by around 6 times at the early stage of liquid injection after approximately 10 pore volumes of gas injection (denoted in Fig. 8 as GPV), but provides a reasonably good estimation at the late stage. For the low-permeability formation (Fig. 8(a)), the conventional simulation algorithm underestimates liquid injectivity at the early stage by about 60 times during injection of liquid after 1 GPV is injected. The liquid injectivity is underestimated by about 120 times if liquid injection is carried out after about 10 GPV. The difference becomes much less obvious at the late stage. In the same injection scenario, a lower-permeability formation experiences a smaller dimensionless pressure drop. One possible explanation is that the collapsed-foam region spreads at a similar speed around the injection well in formations with various permeabilities, while the total relative mobility during liquid injection in the collapsed-foam region is much greater in the lower-permeability formation. This leads to a lower pressure drop and improved liquid injectivity.

The impact of liquid injection rate on the injectivity of liquid after 5 PV gas injection is depicted in Fig. 9. The conventional simulation algorithm falls short in fully capturing this effect, i.e. the shear-thinning behaviour, due to the lack of capability to represent the liquid-fingering and the gas-dissolution processes and their effects on the liquid flow properties in the conventional foam models.

In the high-permeability formation, for liquid injection at $10Q_0$, the peak dimensionless pressure drop measures approximately 370, whereas it is approximately 110 for the case of $0.01Q_0$. The forced-imbibition bank exhibits an extremely shear-thinning behaviour, as reflected by a maximum dimensionless pressure drop only 3.4 times higher. As the injection rate increases by a factor of 1000, the dimensionless pressure drop at long times increases by a factor of approximately 233, indicating the shear-thinning behaviour in the gas-dissolution bank is less obvious (see Fig. 9(c)).

A correction factor for dimensionless pressure drop (DP correction factor) is applied to better represent the difference between the liquid injectivity evaluated by the bank-propagation model and the conventional simulation algorithm as well as the impact of gas and liquid injection rate. The DP correction factor is defined as the ratio of the dimensionless pressure drop calculated from the conventional foam model to that from the bank-propagation model. We present the DP correction factor at the peak dimensionless pressure drop and the one at the late stage, during liquid injection following a time of gas injection.

As shown in Fig. 10(a), the DP correction factor at the peak increases from less than 1 to more than 300 as the injection rate increases; a nearly consistent trend applies to the various formation permeabilities. For a same injection rate, the higher the formation permeability, the smaller the DP correction factor at the peak. This

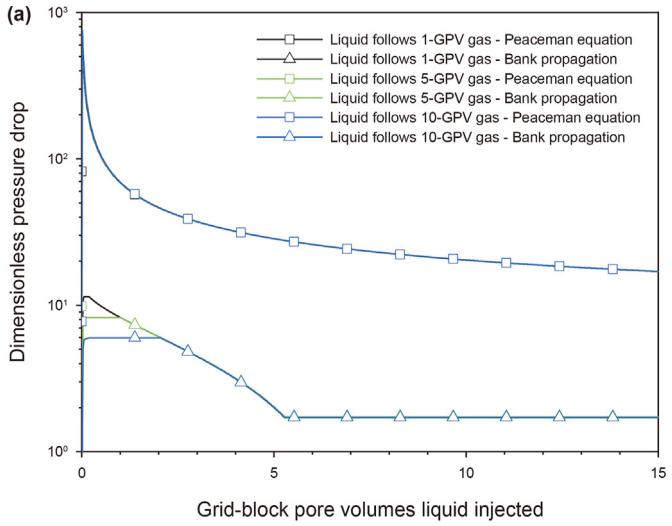

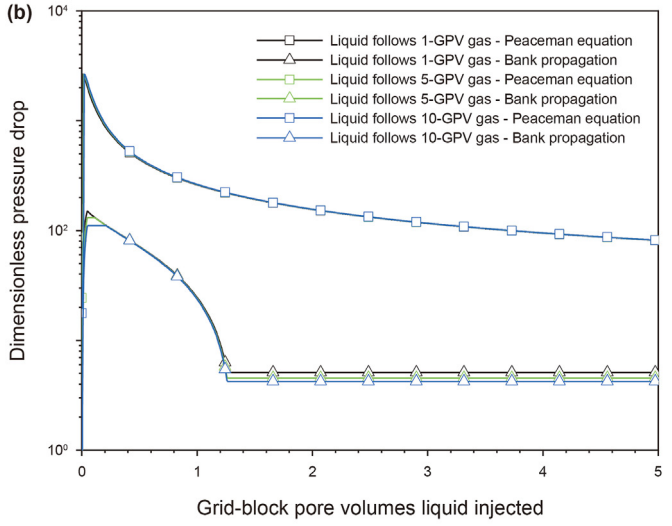

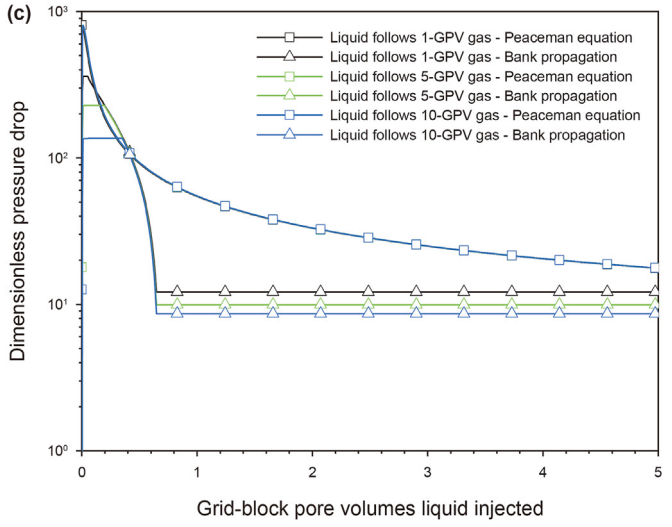

Fig. 8. Liquid injection at volumetric rate $Q_0 = 4.5 \times 10^{-4}$ m^3/(s m) (39 m^3/(day m)) following various amount of gas injection. (**a**) Fontainebleau; (**b**) Berea; (**c**) Bentheimer.

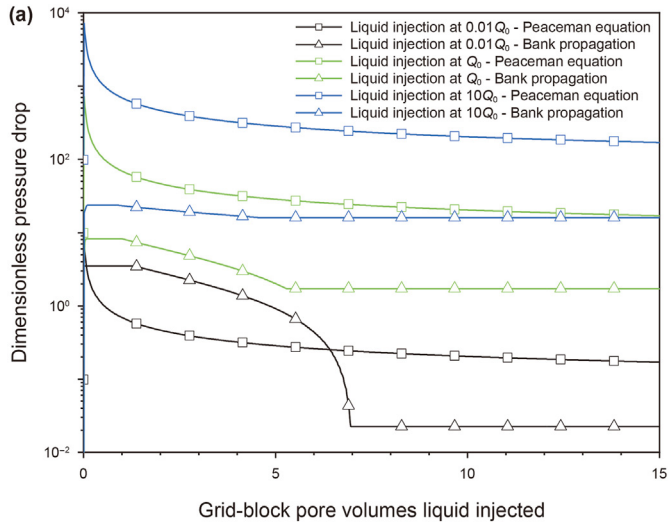

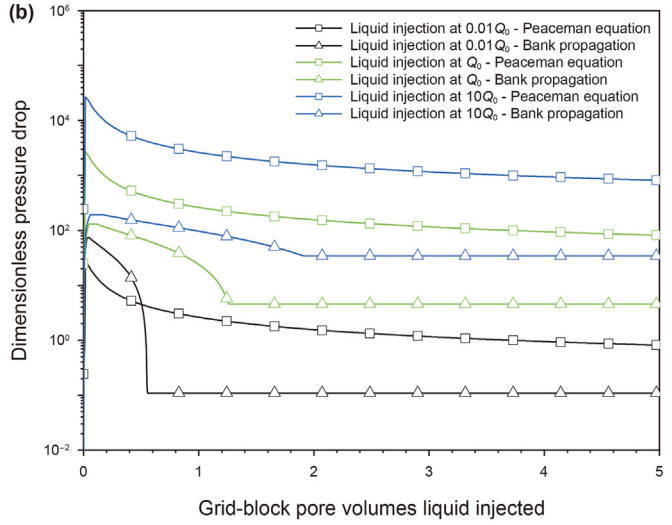

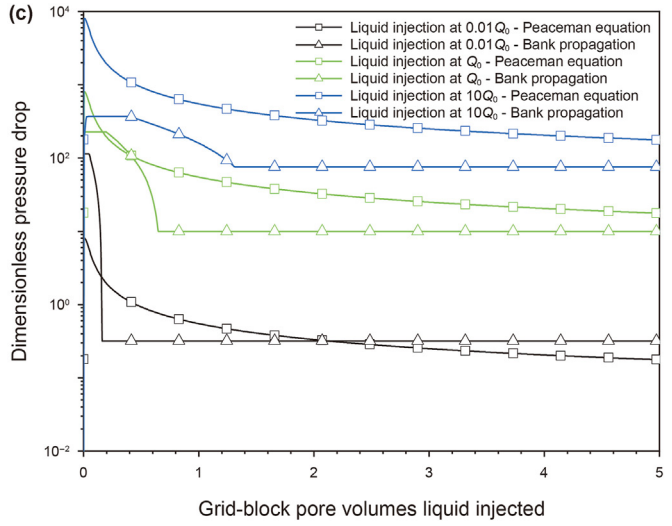

Fig. 9. Liquid injection at various rates following the same amount of gas injection (5 GPV). (**a**) Fontainebleau; (**b**) Berea; (**c**) Bentheimer.

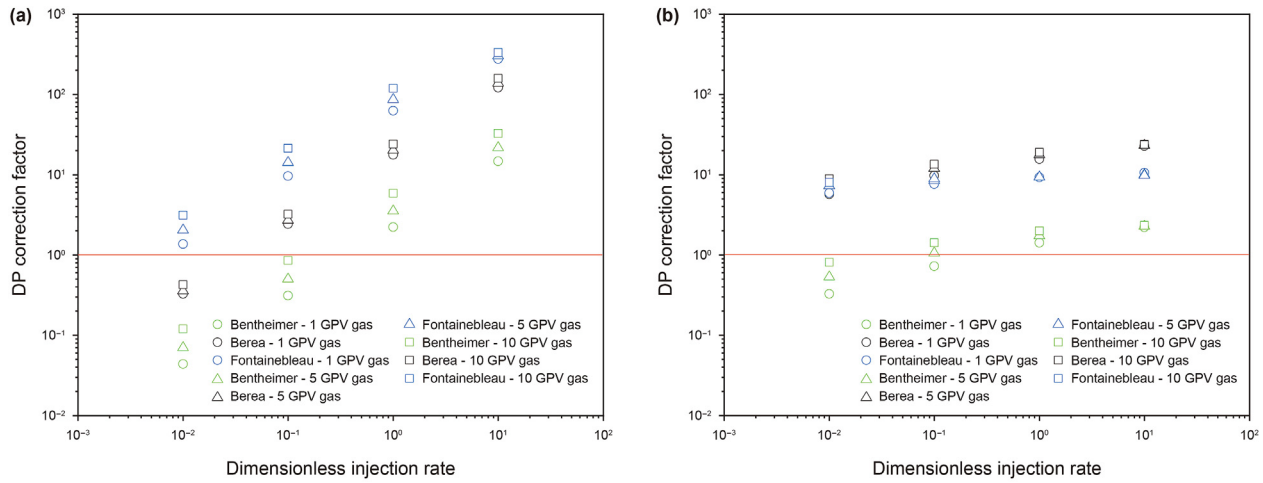

Fig. 10. Correction factor of dimensionless pressure drop. (**a**) Fitting peak dimensionless pressure drop; (**b**) Fitting late stage in dimensionless pressure drop. The dimensionless injection rate is defined as the ratio of the injection rate (Q) to Q_0 (4.5×10^{-4} m^3/(s m) (39 m^3/(day m)).

implies that the conventional foam model overestimates the initial liquid injectivity at relatively low injection rate, and underestimates the initial liquid injectivity more greatly for higher liquid injection rate. In contrast, the liquid injection rate does not have a significant impact on the DP correction factor at the late injection stage (Fig. 10(b)). Especially, the conventional foam model does well in estimating the liquid injectivity at the late stage in the high-permeability formation.

5. Conclusions

The objective of this research is to examine how permeability impacts the flow dynamics during the injection of gas and liquid in a surfactant-alternating-gas foam process and the implications for field application. The main findings and discussion are as follows:

(1) During gas injection following foam in a SAG process, a similar trend in behaviour is observed for all the permeabilities examined: a region of collapsed foam forms and slowly propagates outward from the injection face. In formations with different permeabilities, the collapsed-foam bank spreads with a comparable dimensionless velocity and has a similar total mobility.
(2) When liquid is injected immediately after foam, the flow pattern is similar for various formation permeabilities. However, the gas-dissolution front propagates faster and the plateau value of pressure gradient is lower with higher permeability.
(3) After achieving steady-state foam, when liquid is introduced following a time of gas injection, a similar trend in behaviour is observed for all the permeabilities examined: liquid first rapidly occupies the collapsed-foam area, and subsequently penetrates the foam through fingers. A forced-imbibition bank and a gas-dissolution bank develop beyond the collapsed-foam region near the injection face.
(4) At relatively low liquid injection velocity, a similar trend applies to the banks. The higher the formation permeability, the faster the banks propagate, and the lower the total mobility of the banks.
(5) The conventional simulation algorithm underestimates the initial liquid injectivity at relatively low injection rate, and overestimates the initial liquid injectivity more at higher liquid injection rates. A conventional foam model delivers a reasonable approximation of the liquid injectivity at the late stage in the high-permeability formation, regardless of the liquid injection rate.

CRediT authorship contribution statement

Jia-Kun Gong: Data curation, Formal analysis, Methodology, Writing – original draft. **Yuan Wang:** Formal analysis, Investigation. **Ridhwan-Zhafri B. Kamarul Bahrim:** Formal analysis, Resources. **Raj-Deo Tewari:** Project administration. **Mohammad-Iqbal Mahamad Amir:** Resources, Validation. **Rouhi Farajzadeh:** Formal analysis, Project administration. **William Rossen:** Conceptualization, Methodology, Supervision, Writing – review & editing.

Declaration of competing interest

The authors declare that they have no known competing financial interests or personal relationships that could have appeared to influence the work reported in this paper.

Acknowledgments

This work was supported by the National Natural Science Foundation of China (Grant Nos. U2240210, 52279098), the Natural Science Foundation of Jiangsu Province (Grant No. BK20200525), and the Fundamental Research Funds for the Central Universities (Grant No. B230201021). We express our gratitude to PETRONAS and Shell Global Solution International B.V. for their support of this work.

References

Apaydin, O.G., Kovscek, A.R., 2001. Surfactant concentration and end effects on foam flow in porous media. Transport Porous Media 43, 511–536. https://doi.org/10.1023/A:1010740811277.
Atteia, O., Estrada, E.D.C., Bertin, H., 2013. Soil flushing: a review of the origin of efficiency variability. Rev. Environ. Sci. Biotechnol. 12 (4), 379–389. https://doi.org/10.1007/s11157-013-9316-0.
Bertin, H.J., Apaydin, O.G., Castanier, L.M., et al., 1998. Foam flow in heterogeneous porous media: effect of crossflow. In: SPE/DOE Improved Oil Recovery Symposium. https://doi.org/10.2118/39678-MS.
Boeije, C., Rossen, W.R., 2015. Fitting foam-simulation-model parameters to data: I. Coinjection of gas and liquid. SPE Reservoir Eval. Eng. 18, 264–272. https://doi.org/10.2118/174544-PA.
Cheng, L., Reme, A.B., Shan, D., et al., 2000. Simulating foam processes at high and

low foam qualities. In: SPE/DOE Improved Oil Recovery Symposium. https://doi.org/10.2118/59287-MS.
Computer Modeling Group Ltd, 2006. STARS User's Guide. CMG, Calgary.
Ding, M.C., Li, Q., Yuan, Y.J., et al., 2022. Permeability and heterogeneity adaptability of surfactant-alternating-gas foam for recovering oil from low-permeability reservoirs. Petrol. Sci. 19 (3), 1185–1197. https://doi.org/10.1016/J.PETSCI.2021.12.018.
Farajzadeh, R., Andrianov, A., Zitha, P.L.J., 2010. Investigation of immiscible and miscible foam for enhancing oil recovery. Ind. Eng. Chem. Res. 49 (4), 1910–1919. https://doi.org/10.1021/ie901109d.
Farajzadeh, R., Lotfollahi, M., Eftekhari, A.A., et al., 2015. Effect of permeability on implicit-texture foam model parameters and the limiting capillary pressure. Energy Fuel. 29 (5), 3011–3018. https://doi.org/10.1021/acs.energyfuels.5b00248.
Gong, J., Vincent Bonnieu, S., Kamarul Bahrim, R.Z., et al., 2019. Modelling of liquid injectivity in surfactant-alternating-gas foam enhanced oil recovery. SPE J. 24 (3), 1123–1138. https://doi.org/10.2118/190435-PA.
Gong, J., Vincent Bonnieu, S., Kamarul Bahrim, R.Z., et al., 2020a. Laboratory investigation of liquid injectivity in surfactant-alternating-gas foam enhanced oil recovery. Transport Porous Media 131, 85–99. https://doi.org/10.1007/s11242-018-01231-5.
Gong, J., Vincent Bonnieu, S., Kamarul Bahrim, R.Z., et al., 2020b. Injectivity of multiple slugs in surfactant alternating gas foam EOR: a CT scan study. SPE J. 25 (2), 895–906. https://doi.org/10.2118/199888-PA.
Gong, J., Martinez, W.F., Vincent Bonnieu, S., et al., 2020c. Effect of superficial velocity on liquid injectivity in SAG foam EOR. Part 2: modelling. Fuel 279, 118302. https://doi.org/10.1016/j.fuel.2020.118302.
Heller, J.P., 1994. CO_2 foams in enhanced oil recovery. In: Schramm, L.L. (Ed.), Foams: Fundamentals and Applications in the Petroleum Industry. American Chemical Society, Washington, D.C., pp. 201–234
Hirasaki, G.J., Lawson, J.B., 1985. Mechanisms of foam flow in porous media: apparent viscosity in smooth capillaries. SPE J. 25 (2), 176–190. https://doi.org/10.2118/12129-PA.
Kapetas, L., Vincent Bonnieu, S., Farajzadeh, R., et al., 2017. Effect of permeability on foam-model parameters: an integrated approach from core-flood experiments through to foam diversion calculations. Colloids Surf. A Physicochem. Eng. Asp. 530, 172–180. https://doi.org/10.1016/j.colsurfa.2017.06.060.
Kibodeaux, K.R., Rossen, W.R., 1997. Coreflood study of surfactant-alternating-gas foam processes: implications for field design. In: SPE Western Regional Meeting. https://doi.org/10.2118/38318-MS.
Kovscek, A.R., Radke, C.J., 1994. Fundamentals of foam transport in porous media. In: Schramm, L.L. (Ed.), Foams: Fundamentals and Applications in the Petroleum Industry. American Chemical Society, Washington, D.C, pp. 115–163.
Kuehne, D.L., Ehman, D.I., Emanuel, A.S., et al., 1990. Design and evaluation of a nitrogen-foam field trial. J. Petrol. Technol. 42 (2), 504–512. https://doi.org/10.2118/17381-PA.
Lake, L.W., Johns, R.T., Rossen, W.R., et al., 2014. Fundamentals of Enhanced Oil Recovery. Society of Petroleum Engineers, Richardson.
Le, V.Q., Nguyen, Q.P., Sanders, A.W., 2008. A novel foam concept with CO_2 dissolved surfactants. In: SPE/DOE Symposium on Improved Oil Recovery. https://doi.org/10.2118/113370-MS.
Lee, H.O., Heller, J.P., Hoefer, A.M.W., 1991. Change in apparent viscosity of CO_2 foam with rock permeability. SPE Reservoir Eng. 6 (4), 421–428. https://doi.org/10.2118/20194-PA.
Li, B.F., Zhang, M.Y., Li, Z.M., et al., 2023. Flow characteristics and regime transition of aqueous foams in porous media over a wide range of quality, velocity, and surfactant concentration. Petrol. Sci. 20 (2), 1044–1052. https://doi.org/10.1016/j.petsci.2022.11.014.
Martinsen, H.A., Vassenden, F., 1999. Foam-assisted water alternating gas (FAWAG) process on Snorre. In: European IOR Symposium. https://doi.org/10.3997/2214-4609.201406335.
Matthews, C.S., 1989. Carbon dioxide flooding. In: Donaldson, E.C., Chilingarian, G.V., Yen, T.F. (Eds.), Developments in Petroleum Science. Elsevier, Amsterdam, pp. 129–156.
Moradi-Araghi, A., Johnston, E.L., Zornes, D.R., et al., 1997. Laboratory evaluation of surfactants for CO_2-foam applications at the South Cowden unit. In: International Symposium on Oilfield Chemistry. https://doi.org/10.2118/37218-MS.
Peaceman, D.W., 1978. Interpretation of well-block pressures in numerical reservoir simulation. SPE J. 18, 183–194. https://doi.org/10.2118/6893-PA, 03.
Rossen, W.R., 1996. Foams in enhanced oil recovery. In: Prud'homme, R.K., Khan, S.A. (Eds.), Foams: Theory, Measurements and Applications. Marcel Dekker, New York, pp. 413–464.
Rossen, W.R., Lu, Q., 1997. Effect of capillary crossflow on foam improved oil recovery. In: SPE Western Regional Meeting. https://doi.org/10.2118/38319-MS.
Rossen, W.R., van Duijn, C.J., Nguyen, Q.P., et al., 2010. Injection strategies to overcome gravity segregation in simultaneous gas and water injection into homogeneous reservoirs. SPE J. 15 (1), 76–90. https://doi.org/10.2118/99794-PA.
Schramm, L.L., 1994. Foams: Fundamentals and Applications in the Petroleum Industry. American Chemical Society, Washington, D.C.
Wang, S., Mulligan, C.N., 2004. An evaluation of surfactant foam technology in remediation of contaminated soil. Chemosphere 57 (9), 1079–1089. https://doi.org/10.1016/j.chemosphere.2004.08.019.
Xing, D., Wei, B., McLendon, W., et al., 2012. CO_2-soluble, nonionic, water-soluble surfactants that stabilize CO_2-in-brine foams. SPE J. 17 (4), 1172–1185. https://doi.org/10.2118/129907-PA.
Yaghoobi, H., Heller, J.P., 1996. Effect of capillary contact on CO_2-foam mobility in heterogeneous core samples. In: Permian Basin Oil and Gas Recovery Conference. https://doi.org/10.2118/35169-MS.